Effect of n=1 RMP-driven Turbulence on Ion Pedestal and its role in Adaptive ELM control in KSTAR

S. K. Kim[1,2], R. Shousha[1], S. H. Hahn[3], A. O. Nelson[1], J. Wai[1], S. M. Yang[2], J.-K. Park[2], Y. In[4], J. H. Lee[3], J. Kim[3], and E. Kolemen[1,2*],

[1] *Princeton University, Princeton, U.S.A*

[2] *Princeton Plasma Physics Laboratory, Princeton, U.S.A*

[3] *Korea Institute of Fusion Energy, Daejeon, Korea*

[4] *Ulsan National Institute of Science Technology, Ulsan, Korea*

Introduction

One of the most effective methods to control ELMs is to apply resonant magnetic perturbations (RMPs) using 3D coils [1]. However, this inevitably comes at the considerable expense of global confinement degradation [2] and decreased access to high-performance plasma regimes. In addition, the ELM suppression can be easily lost during discharge due to its narrow operation window.

We report a new adaptive real-time approach to overcome these limitations in a way that optimizes both the pedestal stability and confinement by exploiting the hysteresis [3] in n=1 RMP ELM suppression. Such adaptive control is essential to maximize the plasma performance while also maintaining a stable ELM suppression. Here, we find that RMP-induced ion-scale turbulence during ELM free phase widens the ion pedestal and improves its stability, allowing a higher pedestal pressure and amplified field penetration. This contributes to the fast and stable system control, leading to successful optimization of controlled ELM-free state.

Adaptive ELM control

The real-time adaptive approach in this study detects ELMs from a D_α emission and tries to find the optimum RMP strength or coil current I_{RMP} sufficient to maintain the ELM-free state while small enough to maximize the confinement. The adaptive ELM control experiment (#26004) introduced here is outlined in Fig.1. This control is done by repeating n=1 RMP [4] ramp-up and down until the entry and the loss of ELM suppression are identified, respectively, as shown in Fig.2. Note that H_{98} initially drops from 1.0 to 0.68 after the first ELM suppression. However, the adaptive controller raises the plasma confinement and finally achieved $H_{98} \approx 0.9$, where 60% of initial degradation is recovered. This result is encouraging in that this is close to the ITER target, $H_{98} = 1$.

The fast and successful convergence of adaptive control is mainly due to the decreased RMP strength (I_{IN}) required to enter ELM suppression later in the discharge. I_{IN} for each suppression entry changes as 4.6→3.6→3.5 kA, as seen in Fig.1(a). Because the gap between I_{IN} and I_{OUT} is the discontinuity of this controlled system, decreased I_{IN} reduces the control oscillation so that an optimal RMP strength can

be quickly reached. The schematic diagram Fig.2 illustrates that control convergence will be much delayed without this change in I_{IN}. This is a favorable outcome of the additional edge ion-scale turbulence induced by RMP.

RMP-induced turbulence

The edge turbulence triggered by RMPs is revealed by fluctuation measurements [5-9] after ELM suppression. Fig.3(a) and (b) illustrate contour plots of the integrated coherence strength of electron temperature (δT_{e}) and density (δn_{e}) fluctuations ($k_{\perp}\rho < 1$). Fig.3(c) shows the magnetic field fluctuations (δB_{pol}) at the inner wall. They show an immediate instigation of turbulence as ELM suppression begins. Here, δT_{e} and δn_{e} have strong coherence over the frequency range of 20-100 kHz. δB_{pol} also presents an abrupt increase in the 80-400 kHz range during the same period. Here, the widening of the ion pedestal during 6.3-7.1 s (Fig.3(d)) coincides with the occurrence of edge fluctuations. Therefore, a simultaneous increase in pedestal width and turbulence intensity strongly supports that the ion pedestal is changed due to increased heat diffusivity by ion-scale turbulence. In addition, the edge ExB shearing rate (Fig.3(e)) decreases by the degraded pedestal.

Advantages of widened ion-pedestal on adaptive ELM control

The change in ion pedestal improves the pedestal confinement and stability, which leads to decreasing I_{IN}. Fig.4 illustrates the poloidal beta of pedestal top ($\beta_{\mathrm{p,ped}}$) versus I_{RMP} [10]. The changes to the pedestal from 5.3 to 7.8 s are shown, and the ELMy and suppressed states are marked with grey and orange points, respectively. The contour plot shows the perturbed radial field strength at the pedestal (δB_{r}) from an ideal response calculation using the IPEC code [11]. Here, ELM suppression occurs above a certain δB_{r} threshold, and the ELM free regime is achieved at ~20 G (drawn as a red curve) in this experiment. Fig.4 once again presents the cycle of ELM suppression entry (5.2-6.5 s) → saturation (6.5-7.1 s) → escape (7.1-7.8 s) achieved by varying the RMP strength. At this point, the difference in the trajectories of 5.2-6.5 s and 7.1-7.8 s shows the effect of widened ion-pedestal. In theory, $\beta_{\mathrm{p,ped}}$ should stay under the stability limit to avoid the reappearance of ELM crashes [12]. Stability analysis using the EPED [13] confirms that $\beta_{\mathrm{p,ped}}$ stays below 70% of the stability limit, which improves with increased pedestal width. Therefore, widened pedestal allows for larger $\beta_{\mathrm{p,ped}}$ during the ELM-free phase. Numerical analysis reveals that the stability limit increases by 53% due to ion pedestal broadening. This change in pedestal stability is presented in Fig.4 as the purple and blue lines. With such improvement, the lower limit of the suppression regime (I_{OUT}) is expanded, and I_{RMP} can decrease to 3.6 kA, allowing for further $\beta_{\mathrm{p,ped}}$ increase. If there is no such effect, ELMs will return at higher I_{RMP} > 5 kA, and most of the pedestal recovery shown in 7.1-7.8 s will be lost.

Large poloidal beta near the pedestal amplifies the edge plasma response and field penetration, as shown in Fig.4. Because $\beta_{\mathrm{p,ped}}$ at the moment of ELM suppression loss is much higher than at the entry phase, the

same δB_r can be obtained with a smaller I_{RMP}. This leads to a lower I_{IN}, making access to a second ELM suppression regime easier. Fig.4 clearly shows that I_{IN} decreases from 4.9 to 3.6 kA at 7.7 s. As ELMs re-occur near I_{RMP} ~ 3.3 kA, it is possible to re-enter the ELM free state by raising I_{RMP} by only 0.3 kA. Consequently, fast and stable confinement optimization using adaptive RMP control becomes feasible.

Linear gyrokinetic simulation

Linear analysis for drift wave instabilities using CGYRO [14] reveals that the occurrence of edge turbulence can be correlated to the reduced ExB shearing rate. Fig.5 shows the spectra of Bohm normalized linear growth rate and real frequency for the most unstable modes vs. the normalized bi-normal wave number $k_\perp \rho$. This calculation is performed at the pedestal top. The simulation indicates that the ITG/TEM hybrid mode can occur during the ELM suppression phase (6.6-7.7 s) mainly due to decreased ExB shearing rate ($\gamma_{E\times B}$) shown by the dashed lines in Fig.5 (b). The simulation results show that ion thermal diffusion can be increased with these unstable modes, supporting the idea of ion pedestal broadening by turbulence. However, recent nonlinear studies have shown that RMP-induced turbulence can be accurately described only with the inclusion of non-linearity [15] and non-locality [16]. In addition, such turbulence is known [5,17] to have a significant effect on electron channels rather than ion pedestal, which is inconsistent with this observation. In the future, nonlinear gyrokinetic studies, including RMP effects, will shed further light on this issue.

Conclusion

In conclusion, an adaptive approach for ELM control is successfully demonstrated its potential to simultaneously achieve both optimized plasma confinement and stable ELM-free state using RMPs is explained. This is made possible by decreased I_{IN} during adaptive control. This favorable change is the outcome of ion-scale turbulence transport induced naturally by RMPs. Consequently, the controller successfully converged to an optimal RMP strength, illuminating a new strategy to achieve high confinement ELM-free plasmas in ITER.

Acknowledgement

The authors would like to thanks KSTAR team. This material was supported by the U.S. Department of Energy, under Awards DE-SC0020372. This research was also supported by R&D Program of "KSTAR Experimental Collaboration and Fusion Plasma Research (EN2021-12)" through the Korea Institute of Fusion Energy (KFE) funded by the Government funds.

References

[1] T. E. Evans et al., PRL 92, 23 (2004).
[2] T. E. Evans et al., NF 48, 2, 024002 (2008).
[3] F. Laggner et al., NF 60, 7, 076004 (2020).
[4] Y. M. Jeon et al., PRL 109, 3 (2012)
[5] S. Mordijck et al., POP 19, 2, 024504 (2012)
[6] G. R. McKee et al., NF 53, 11, 113011 (2013)
[7] R. Nazikian et al., PRL 114, 10 (2015).
[8] N. Vianello et al., PPCF 57, 1, 014027 (2015)
[9] J. Lee et al., NF 59, 6, 066033 (2019).
[10] J.-K. Park et al., NP 14, 12, 1223 (2018).

[11] J.-K. Park et al., POP 14, 5, 052110 (2007).

[12] P. B. Snyder et al., NF 47, 8, 961 (2007).

[13] P. B. Snyder et al., POP 16, 5, 056118 (2009).

[14] L. Cui et al., NF 57, 11, 116030 (2017

[15] R. Hager et al., POP 27, 6, 062301 (2020).

[16] S. Taimourzadeh et al., NF 59, 046005 (2019)

[17] C. Sung et al., POP 24, 11, 112305 (2017).

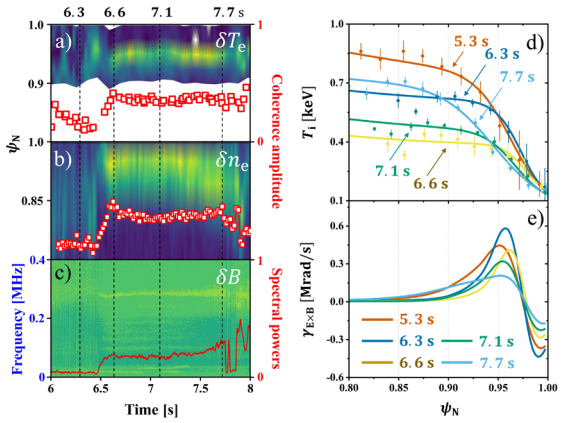

Figure 3. Contours of mode coherence in edge fluctuation measured from (a) ECEI and (b) BES vs time and ψ_N. Integrated coherence amplitude of fluctuations is drawn as red squares. (c) Contours of magnetic spectrum measured at inner wall vs time and frequency. Integrated spectral power of measured fluctuation is shown as red line. Profiles of (d) Ion pedestal $T_{i,ped}$ and (e) ExB shearing rate for t = 5.3-7.7 s.

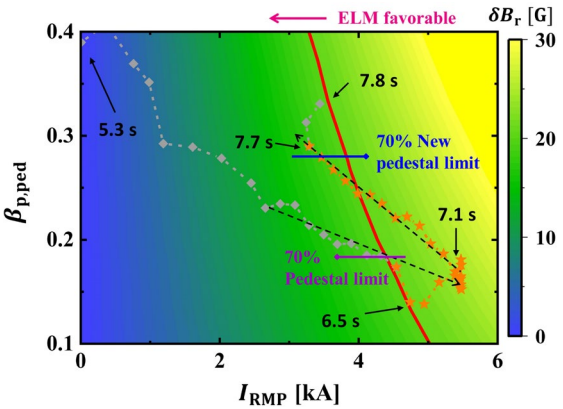

Figure 4. Contours of δB_r at pedestal region from ideal response calculation vs I_{RMP} and pedestal poloidal beta $\beta_{p,ped}$. Experimental δB_r value for ELM suppression entry is drawn as red curve. The time traces of #26004 discharge from 5.0 to 7.8 s are marked as grey (ELMy) and orange dots (ELM-free). 70% of ideal pedestal stability limits predicted by experimental parameters, profiles, and ideal MHD code are drawn as purple (before ELM suppression entry) and blue (after entry).

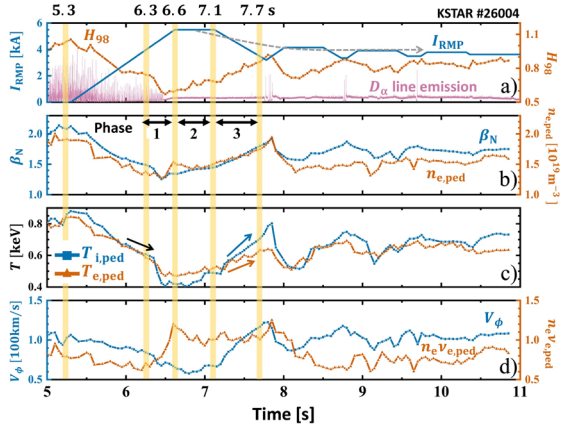

Figure 1. Time traces of discharge #26004 with adaptive ELM control using n = 1 RMP. (a) RMP coil current I_{RMP} (blue), plasma confinement scaling H_{98} (orange), and D_α emission near the outer strike point (pink). (b) Normalized beta β_N (blue) and density pedestal height $n_{e,ped}$ (orange). (c) Pedestal height of ion $T_{i,ped}$ (blue) and electron $T_{e,ped}$ (orange). (d) Toroidal carbon velocity at pedestal $V_{\phi,ped}$ (blue) in co-Ip direction and energy exchange coefficient $nv_{e,ped}$ on pedestal (orange). Grey dashed line in (a) denotes the change of I_{IN}.

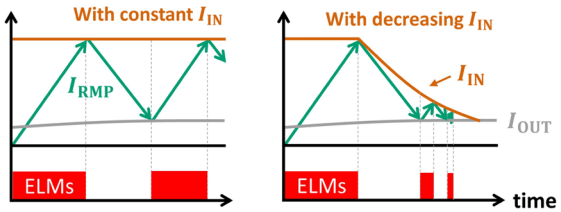

Figure 2. Schematic diagram of adaptive ELM control approach and difference in time traces of RMP strength with and without decreasing I_{IN}.

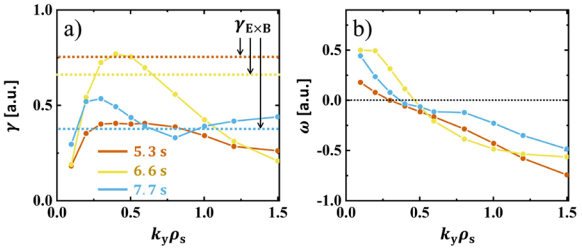

Figure 5. The (a) linear growth rate and (b) real frequency of the drift wave instabilities for the three interested time ranges at pedestal centre. The dashed line in (a) are ExB shearing rate ($\gamma_{E\times B}$) at each time range.